Research Square

Preprints are preliminary reports that have not undergone peer review.
They should not be considered conclusive, used to inform clinical practice,
or referenced by the media as validated information.

Nickel Carbon Composite With Carbon Nanotubes for Efficient Electromagnetic Wave Absorption

Yun Qiu
Shaanxi University of Science and Technology
Haibo Yang (yanghaibo@sust.edu.cn)
Liang Ma
Xianyang Non-metallic Mineral R & D Institute Co.,Ltd
Ying Lin
Shaanxi University of Science and Technology
Hanwen Zong
Shaanxi University of Science and Technology
Bo Wen
Shaanxi University of Science and Technology
Xiaoyu Bai
Shaanxi University of Science and Technology
Mengqi Wang
Shaanxi University of Science and Technology

Research Article

Keywords: Metal organic framework; nickel, carbon nanotubes, electromagnetic wave absorption

Posted Date: June 9th, 2020

DOI: https://doi.org/10.21203/rs.3.rs-33498/v1

License: This work is licensed under a Creative Commons Attribution 4.0 International License.
Read Full License

Abstract

Nickel carbon composite with carbon nanotubes (Ni-C/CNTs) has been fabricated by pyrolysis the mixture of nickel-based metal organic framework (Ni-MOF) and melamine. The resultant Ni-C/CNTs composite is assembled from one-dimensional (1D) CNTs and three dimensional (3D) spherical Ni-C composite. Besides, the Ni-C/CNTs composite contains abundant nitrogen(N) dopants that contributes to defect dipole polarization. The diameter and length of CNTscan beeffected by changing the mass ratio of Ni-MOF and melamine. The optimizedNi-C/CNTs composite exhibits reflection loss of -55.1 dB at 10.56 GHz, and the effective absorbing bandwidth (reflection loss < -10 dB) is 11.2 GHz (6.0-17.2 GHz)with the thickness range of 1.5-4.0 mm, when the mass ratio of Ni-MOF: melamine is 1: 2. These results indicate that the mixed 1D-3D hierarchical architecture synergistically improves electromagnetic wave absorption properties. This strategy willcontribute for fabricating the carbon hybrid network consisting of metal organic frameworks derived metal/carbon hybrid and CNTs for electromagnetic wave absorption.

1. Introduction

Recently, with the popularity of local area networks, radar systems, as well as the extensive application of computers, mobile phones and other electronic equipment, the problem of electromagnetic (EM) interference tends to be serious. Therefore, it is very important to effectively suppress and reduce EM radiation. EM wave absorbing materials can absorb and attenuate the incident EM wave, which provides an effective solution for the EM wave pollution [1, 2]. With the continuous development of research and application of EM absorbing materials, the types of materials tend to be diversified and complicated [3, 4]. The new EM absorbents need to to satisfy the characteristics of low thickness, lightweight, wide absorption frequency bandwidth and strong absorption performance [5, 6].

Metal organic frameworks (MOFs) consisting of metal ions and organic ligand possess the advantages of tunable porosity and controllable microstructure [7]. Over the past decade, MOFs and their derivatives (metal oxide and metal carbon composites) have received considerable attention in many applications [8–10]. Magnetic metal/carbon composites derived from MOFs inherit the morphology and the pore structure of original MOFs. Besides, magnetic particles are wrapped by carbon and uniformly dispersed in carbon matrix [11–13]. Especially in the field of EM absorption, the MOFs containing magnetic metal ions (Fe^{3+}, Co^{2+} and Ni^{2+}) derived metal/carbon composites have both magnetic loss and electric loss, which provide multiple ways for the attenuation of EM waves. For example, Peng et al. [14] fabricated flower-like Fe_3C/C and Fe_3C/Fe/C composites by carbonization of MIL-101 with a maximum reflection loss (RL_{max}) of -39.43 dB and − 20.31 dB at 2 mm, respectively. Wang and co-workers [15] used Co-MOF-74 as the precursor to fabricate porous Co-C core-shell nanocomposites with RL_{max} of -62.12 dB at 11.85 GHz. Ni/C composite prepared by pyrolyzed nickel based MOF at high temperatures showed a strong RL of -86.8 dB at the thickness of 2.7 mm [16]. Nevertheless, for MOFs derived metal/carbon composites, it is still difficult to achieve excellent EM wave absorption performances with low-thickness regions and broad effective absorption bandwidth (EAB).

1D CNTs have unique hollow tubular structure, large aspect ratio, prominent electrical and mechanical properties [17, 18], which make them have a good application prospect in EM wave absorbing materials. However, the weak impedance matching limits the practical application of CNTs as EM wave absorbent [19, 20]. Therefore, combining CNTs with magnetic materials is one of the effective strategies to get desirable EM wave absorbent. However, the CNTs require being pretreatment by complicated chemical process before they can be combined with other materials [21, 22]. Studies on utilizing facile synthesis methods to prepare the composites of CNTs and magnetic materials are rarely reported.

The structure of EM absorbing material is the key of absorbing EM wave. Many studies have been proved that the mixed hierarchical architecture could integrate the advantages from different structural units [23, 24]. Herein, in this work, 3D Ni-MOF microsphere is used as the precursor, and melamine is used as initiator for the growth of 1D CNTs. After pyrolyzing the composite of melamine/Ni-MOF at argon atmosphere, Ni-C/CNTs composite is obtained. The Ni-MOF microspheres are transformed into Ni-C composite and the generated Ni nanoparticles can also be used as the catalyst for CNTs growth. As a result, some Ni nanoparticles are encapsulated in the tips of the CNTs and the rest are embedded in the carbon shell derived from Ni-MOF. The as-synthesized Ni-C/CNTs composite presents superior EM wave absorbing performances. The RL_{max} is -55.1 dB at 10.56 GHz with the EAB of 11.2 GHz (6.0-17.2 GHz) at absorber thickness below 4.0 mm.

2. Experimental Section

2.1 Materials. Nickel nitrate hexahydrate ($Ni(NO_3)_2$•$6H_2O$, 98%), benzene-1, 3, 5-tricarboxylic acid (H_3BTC, 98%), melamine (99%), polyvinylpyrrolidone (PVP-K30, GR), ethanol (99.7%) and N, N-dimethylformamide (DMF, 99.5%) were purchased from Sinopharm Chemical Reagent Co., Ltd.

2.2 Synthesis of Ni-MOF. Ni-MOF was synthesized by solvothermal method similar to the previous report [25]. 864 mg of $Ni(NO_3)_2$·$6H_2O$, 300 mg H_3BTC and 3 g PVP-K30 were mixed with 60 mL DMF and stirred until the solution became light green transparent. Then it was sealed into a 100 mL Teflon-lined stainless-steel autoclave and maintained at 150 ^oC for 10 h. The obtained green precipitate was washed with ethanol and dried at 60 ^oC for 12 h.

2.3 Synthesis of Ni-C/CNTs composite. 400 mg of as-prepared Ni-MOF was mixed with various amounts of melamine (400 mg, 800 mg and 1200 mg) in 100 mL ethanol and stirred for 12 h at 25 ^oC. After that, the suspension was dried at 60 ^oC in air until the solvent completely evaporated. Afterward, it was firstly pyrolyzed at 550 ^oC for 3 h with heating rate of 2 $^oC\ min^{-1}$ and then subsequently at 700 ^oC for 3 h with a heating rate of 3 $^oC\ min^{-1}$. The obtained Ni-C/CNTs composites were recorded as Ni-C/CNTs-1, Ni-C/CNTs-2 and Ni-C/CNTs-3, respectively. As a contrast, the pure Ni-MOF was also pyrolyzed at the same conditions, and it was named as Ni/C composite.

2.4 Characterization. The crystal structure of samples was investigated by X-ray diffraction (XRD, D8 Advance, Germany). The morphology of products was characterized by field-emission scanning electron microscope (FE-SEM, Hitachi, S-4800) and transmission electron microscope (TEM, JEM-2100). Raman

spectra (Raman, DXRxi) was used to study the graphitization degree of samples. The surface composition of composites was performed using X-ray photoelectron speatra (XPS, AXIS SUPRA).

2.5 Performance Measurements. The complex permittivity ε_r ($\varepsilon_r = \varepsilon' - j\varepsilon''$) and permeability μ_r ($\mu_r = \mu' - j\mu''$) of samples were measured by vector network analyzer (VNA, HP8720ES, Agilent, USA) in the range of 2–18 GHz using the coaxial method. Before testing, the mixture containing 30 wt% the as-prepared materials (Ni/C, Ni-C/CNTs-1, Ni-C/CNTs-2 and Ni-C/CNTs-3) and 70 wt% wax was uniformly mixed at 80 ^{o}C and then pressed into a toroidal ring (outer diameter: 7.0 mm, inner diameter: 3.04 mm and thickness: 3.0 mm).

3. Results And Discussion

The preparation process of Ni-C/CNTs composite is schematically illustrated in Scheme 1. The microspherical Ni-MOF is prepared by solvothermal reaction which is used as precursor to prepare Ni-C/CNTs composites. The precursor is mixed with melamine and pyrolysed by two-stage programmed heating process. The melamine is transformed to g-C_3N_4 at 550 ^{o}C for 3 h under argon atmosphere through its poly-addition and thermo-polymerization [26]. Then it permeates into the Ni-MOF microspheres. Finally, metal cations are reduced to metal nanoparticles and can be used as catalysts to facilitate the formation of CNTs after further increasing the temperature to 700 ^{o}C for 3 h. As a result, the Ni-C/CNTs composite is obtained.

The morphology of Ni/C and Ni-C/CNTs composites are observed by FE-SEM. The Ni/C composite inherits the spherical structure of Ni-MOF precursor, as exposed in Fig. 1(a). Without the melamine participating in the reaction, CNTs cannot be generated. SEM images of Ni-C/CNTs composites are displayed in Fig. 1(b-d). Apparently, the diameter and length of CNTs vary with the amount of melamine. Ni-C/CNTs composites are composed of microspheres linked with plenty of flexible nanotubes.

As observed in TEM images of Fig. 2(a-d), Ni-MOF has evolved into Ni/C composite with the initial spherical structure maintained, and nickel ions in Ni-MOF are transformed into nickel nanoparticles, which are embedded in carbon shell. Under pyrolysis process under argon atmosphere, PVP and organic ligands of H_3BTC are converted into carbon. The TEM images for representative sample of Ni-C/CNTs-2 composite as shown in Fig. 2(e-g). it consists of Ni-C composite and CNTs with Ni nanoparticles encapsulated in nanotubes. The generated Ni nanoparticles could be regarded as the catalyst to promote the conversion of melamine into CNTs. HR-TEM images (Fig. 2(h)) for a single Ni nanoparticle reveals a clear lattice fringes of 0.2 nm, corresponding to the (111) plane of cubic metallic Ni. Evidently, such Ni-C/CNTs composite with hierarchical hybrid nanoarchitectures may be beneficial to enhancing the EM wave transfer capability.

The phase identification of resultant Ni-C/CNTs composites are performed via XRD patterns. As for Ni/C composite,

peaks appeared at about 2θ = 41.8°, 47.5° and 62.1° can be assigned to (100), (101) and (102) planes of carbon (JCPDS No.80 − 0004) [27, 28], respectively. The diffraction peaks at 2θ = 44.5°, 51.8° and 76.4° matched well with (111), (200) and (220) planes of metal Ni with face-centered cubic (fcc) structure (JCPDS No.04-0805), respectively, indicating that Ni^{2+} of Ni-MOF precursor have been reduced into Ni particles by reacting with carbon [29]. After melamine participates in the reaction, a broad peak at approximately 2θ = 25° is the (002) peak of graphitic carbon materials [30]. Diffraction peaks of metallic nickel for Ni-C/CNTs composites are bigger than those of Ni/C composite, implying the better crystallinity of cubic metallic nickel.

The relative graphitization degree of carbon and carbon nanotubes in these composites are discerned by Raman spectra. Two typical peaks located at ~ 1350 and ~ 1590 cm^{-1} present the so-called D band and G band that reveals the characteristic of disordered and graphitic carbon, respectively [31]. The relative graphitization degree of carbon materials is evaluated by the intensity ratio of D and G band (I_D/I_G) [32]. Obviously, the values of I_D/I_G for Ni/C, Ni-C/CNTs-1, Ni-C/CNTs-2, and Ni-C/CNTs-3 composites are calculated to be 1.044, 1.02, 0.9949, and 0.9949, respectively, suggesting the similar graphitization degree.

XPS measurement for the representative Ni-C/CNTs-2 composite is conducted to investigate the element valence state of material. The wide scan XPS spectrum (Fig. 5(a)) verifies the existence of C, N, O, and Ni elements. Figure 5(b) exhibits five fitting peaks with binding energies at 283.92, 284.6, 285.18, 286.52, and 288.71 eV assigned to C = C, C-C, C-N, C-O, and O-C = O groups, respectively [33, 34]. Three peaks at 398.19, 400.17, and 402.49 eV of the high-resolution N 1 s spectrum (Fig. 5(c)) is related to the pyridinic N, pyrrolic N and graphitic N, respectively [35], suggesting that N atoms have been incorporated in the carbon substrate. Theoretically, both pyridinic N and pyrrolic N are important to improve the dipolar relaxation losses, and graphitic N is good for improving conduction loss [36]. In Fig. 5(d), the XPS spectrum of Ni 2p displays two shake-up satellites and two primary peaks at the binding energy of 854.08 and 871.25 eV, corresponding to the Ni $2p_{3/2}$ and Ni $2p_{1/2}$ for metallic Ni, respectively [16, 37].

Both ε_r and μ_r are the basis for judging the absorbing performance of the wave absorber. The real parts (ε' and μ') represent the storage capability and the imaginary parts (ε" and μ") are related the dissipation ability of electric and magnetic energy [38]. As discovered in Fig. 6, the content of melamine plays an important role in modifying the EM parameters of Ni/C composite. From Fig. 6(a), the ε' values reduce as the frequency increases, roughly obeying the frequency dispersion behavior [39–42]. The ε' values of Ni/C composite are enhanced by doping CNTs, which may be caused by the polarization of interfacial and dipole. The ε' values of Ni-C/CNTs-3 are highest among the samples, which suggests highest energy storage and polarization action. The ε" curves (Fig. 6(b)) show similar trend with ε' curves and the ε" values for Ni-C/CNTs composites (Ni-C/CNTs-1, Ni-C/CNTs-2 and Ni-C/CNTs-3) are bigger than those of Ni/C composite at 2–11 GHz. Therefore, CNTs can significantly change the dielectric constant of Ni-C composite. Besides, the downward tendency for Ni-C/CNTs composites are more obvious than that of Ni/C composite indicating that the former can produce more electric dipoles [43]. In Fig. 6(d), the μ' values

of all composites exhibit decrease (2-6.2 GHz) at first, then increase, and last decrease with increasing frequency. It can be observed from Fig. 6(e) that the μ" values for Ni-C/CNTs composites are higher than those of Ni/C composite at the frequencies of 9–18 GHz. The $\tan\delta_\varepsilon = \varepsilon''/\varepsilon'$ and $\tan\delta_\mu = \mu''/\mu'$ values are used to characterize the dielectric loss and magnetic loss ability of absorbers. Besides, it should be noted that in Fig. 6(c, f) the values of $\tan\delta_\varepsilon$ in 2–11 GHz are larger than $\tan\delta_\mu$ values, while in high frequency region this phenomenon is contrast, suggesting that the dielectric loss and magnetic loss are the dominated electromagnetic attenuation loss mechanism for the obtained Ni/C and Ni-C/CNTs composites at low frequency and high frequency range, respectively.

The polarization relaxation process of materials has a great influence on dielectric loss. The Cole-Cole curves of simples are presented in Fig. 7. The relationship of ε' and ε" satisfies the following Formula [44]:

$$(\varepsilon' - \frac{\varepsilon_s+\varepsilon_\infty}{2})^2 + (\varepsilon'')^2 = (\frac{\varepsilon_s-\varepsilon_\infty}{2})^2 \qquad (1)$$

where ε_s refers to the static permittivity. ε_∞ presents relative dielectric permittivity at the high-frequency limit. One semicircle appears in the ε'-ε" diagram corresponds to a polarization relaxation process, suggesting a Debye relaxation process. The multiple semicircles in Cole-Cole plot manifests the existence of multiple relaxation processes under microwave irradiation. This phenomenon is caused by dipole polarization relaxation and interfacial polarization relaxation [44]. Defects such as doped elements (N and O) in carbon nanotubes and carbon skeletons act as jumping centers to endow electrical dipoles in composites, resulting in stable dipole polarization relaxation. The accumulation of interfacial charges between Ni nanoparticles, C and CNTs lead to interfacial polarization. The straight line at the end of Cole-Cole curves is related to the conduction loss that mainly comes from C, CNTs and Ni particles.

The magnetic loss is also important for absorbing the EM waves. Generally, the magnetic loss mainly comes from domain wall resonance, hysteresis loss, and eddy current loss [45]. Domain wall resonance loss and hysteresis loss always occur at low frequency [46]. If the values of $C_0 = \mu''(\mu')^{-2}f^{-1}$ keep constant with the increase of frequency, the eddy current loss contributes to magnetic loss. Contrarily, if the values of C_0 change a lot, the magnetic loss mainly originates from natural resonance and exchange resonance [47]. The values of C_0 for all composites are investigated in Fig. 8. Obviously, C_0 curves of composites fluctuate over the entire frequency range, manifesting that natural resonance and the exchange resonance dominate the magnetic loss.

The RL values are defined by the following equations [22]:

$$\mathrm{RL}(d\mathrm{B}) = 20\log\left|\frac{Z_{in}-Z_0}{Z_{in}+Z_0}\right| \qquad (2)$$

$$Z_{\mathrm{in}} = Z_0\sqrt{\frac{\mu_r}{\varepsilon_r}}\tanh\left(j\frac{2\pi fd}{c}\sqrt{\mu_r\varepsilon_r}\right) \qquad (3)$$

where Z_{in} denotes the normalized input impedance and Z_0 is the impedance of free space, respectively, *f* is the EM frequency, *d* is the thickness of the absorber, c is 3×10^8 m/s. Particularly, when the RL≤ -10 dB, 90% of incident EM wave will be attenuation. Figure 8 exhibits three dimension and two dimension curves of RL for simples at 1.5-4.0 mm. The RL_{max} value of Ni/C composite is -21.7 dB at 8.6 GHz when the matching thickness is 4.0 mm (Fig. 9(a, e, i)). For the Ni-C/CNTs-1 composite (Fig. 9(b, f, j)), the RL_{max} value of -24.1 dB at 2.5 mm is obtained at 10.9 GHz. Besides, when the thickness is 1.7 mm, the superior EAB is 5.7 GHz (12.3–18 GHz) at the corresponding RL_{max} value of -21.3 dB (Fig. 9(f)). As for Ni-C/CNTs-2 composite, the RL_{max} value is -55.1 dB at 10.56 GHz at 2.5 mm (Fig. 9(c, g, k)). Moreover, by changing the thickness from 1.5 mm to 4.0 mm, the EAB reaches 11.2 GHz (6.0-17.2 GHz). However, the RL_{max} value of Ni-C/CNTs-3 composite is only − 17.5 dB at 13.6 GHz with a thickness of 1.5 mm (Fig. 9(d, h, l)). Overall, CNTs can effectively improve the EM wave absorption properties of Ni-C composites.

Impedance matching is one of important parameters to determine the EM absorption properties. When the surface resistance of absorber is close to the resistance of free space ($|Z_{in}/Z_0| = 1$), the external EM wave penetrate the absorber. Figure 10 compares the $|Z_{in}/Z_0|$ values of Ni/C and Ni-C/CNTs composites with a constant sample thickness of 2.5 mm. Apparently, the $|Z_{in}/Z_0|$ values of Ni-C/CNTs-2 composite is closest to 1, which indicates that the Ni-C/CNTs-2 composite has best impedance matching compared with other composites. Accordingly, the RL_{max} of -55.1 dB is achieved for Ni-C/CNTs-2 composite at the same frequency when $|Z_{in}/Z_0| = 1.0$, which satisfies the near zero reflection condition.

Table 1 listed microwave absorption properties of other nickel based materials in the previous references [48–52]. The EM wave absorption ability of Ni-C/CNTs-2 composite outperform many nickel based materials according to combination of the filler loading, thickness, EAB, as well as RL.

According to the above analysis, the feasible EM wave absorption mechanism of Ni/CNTs composite could be attributed to the following aspects, as shown in Scheme 2. Firstly, suitable impedance matching is a prerequisite for EM waves to enter the material and then be attenuated. Secondly, the accumulation of space charges at multiple interfaces among paraffin, Ni nanoparticles, carbon, and CNTs cause interface polarization. Besides, these heterogeneous interfaces also facilitate multiple scattering and reflection of incident EM waves. Thirdly, Ni nanoparticles and carbon core-shell structure derived from Ni-MOF provides magnetic loss and dielectric loss. And the CNTs catalyzed by Ni particles are beneficial to the improvement of the conduction loss and provide an effective way for electronic hopping and migration. Finally, plentiful functional groups N doped defects in Ni-C/CNTs composites generate amount of dipoles, which act as polarized centers to attenuate incident EM waves. Therefore, the excellent microwave absorption ability of the Ni-C/CNTs composite is ascribed to the good impedance matching as well as the synergistic effect of magnetic and dielectric loss.

Table 1
EM absorption properties of some typical nickel based materials in the previous references

Materials	Filler loading (wt%)	Thickness (mm)	RL max (dB)	EAB (GHz)	Refs.
SiC/Ni/NiO/C	20	4.0	-50.52	2.8	[48]
Ni/TiO_2/C	60	1.4	-39.91	–	[49]
Ni@ppy	27	5.0	-48.00	3.8	[50]
$Ti_3C_2T_X$/Ni-spheres	50	1.5	-47.06	3.6	[51]
Ni/NiO/Cu@C	10	3.2	-38.1	< 1.0	[52]
Ni-C/CNTs – 1	30	1.7	-21.3	5.7	This work
Ni-C/CNTs – 2	30	2.5	-55.1	2.6	This work

4. Conclusions

In summary, Ni-C/CNTs composites were prepared via calcining the mixture of Ni-MOF microspheres and melamine through two-stage programmed heating process, which does not require complicated chemical treatment to combine Ni/C composite with CNTs. Meanwhile, each CNT tip is capped with Ni@C core-shell particle, and the spherical Ni/C composite is composed of many Ni@C core-shell particles, which reduce the oxidation or corrosion by air or acid. The as-synthesized Ni-C/CNTs composite exhibits strong EM wave absorption of -55.1 dB with thickness of 2.5 mm and wide EAB 11.2 GHz (6.0-17.2 GHz) as the thickness varies from 1.5 mm to 4.0 mm. This work is expected to pave a way to construct novel materials for EM wave absorption.

Declarations

Conflict of interest

The authors declare that they have no conflict of interest.

Acknowledgements

This work is supported by the National Natural Science Foundation of China (Grant No. 51772177), the Shaanxi Science & Technology Co-ordination & Innovation Project of China (Grant No. 2017TSCXL-GY-08-05) and the Science Fund for Distinguished Young Scholars of Shaanxi Province (Grant No. 2018JC-029).

References

1. Liu QH, Cao Q, Bi H, et al. CoNi@SiO_2@TiO_2 and CoNi@Air@TiO_2 microspheres with strong wideband microwave absorption. Adv Mater. 2016;28:486-+.
2. Liu J, Zhang HB, Sun RH, et al. Hydrophobic, flexible, and lightweight MXene foams for high-performance electromagnetic-interference shielding. Adv Mater. 2017;29:1702367.
3. Li JJ, Yang S, Jiao PZ, et al. Three-dimensional macroassembly of hybrid C@CoFe nanoparticles/reduced graphene oxide nanosheets towards multifunctional foam. Carbon.

2020;157:427–36.

4. Green M, Chen XB. Recent progress of nanomaterials for microwave absorption. Journal of Materiomics. 2019;5:503–41.
5. Liang LY, Yang RS, Han GJ, et al. Enhanced electromagnetic wave-absorbing performance of magnetic nanoparticles-anchored 2D $Ti_3C_2T_x$ MXene. ACS Appl Mater Inter. 2019;12:2644–54.
6. Wang Y, Gao X, Wu XM, et al. Facile synthesis of Mn_3O_4 hollow polyhedron wrapped by multiwalled carbon nanotubes as a high-efficiency microwave absorber. *Ceram Int* 2020 46: 1560–1568.
7. Zhu BJ, Liang ZB, Xia DG, et al. Metal-organic frameworks and their derivatives for metal-air batteries. Energy Storage Materials. 2019;23:757–71.
8. Suh MP, Park HJ, Prasad TK, et al. Hydrogen storage in metal-organic frameworks. Chem Rev. 2012;112:782–835.
9. Yang WP, Li XX, Li Y, et al. Applications of metal-organic-framework-derived carbon materials. *Adv Mater* 2019 31: 1804740.
10. Zhang L, Wu HB, Madhavi S, et al. Formation of Fe_2O_3 microboxes with hierarchical shell structures from metal-organic frameworks and their lithium storage properties. *J Am Chem Soc* 2012 **134**: 17388–17391.
11. Wang YQ, Wang HG, Ye JH, et al. Magnetic CoFe alloy@C nanocomposites derived from ZnCo-MOF for electromagnetic wave absorption. *Chem Eng J* 2020 383: 123096.
12. Qiu Y, Lin Y, Yang HB, Wang L, et al. Hollow Ni/C microspheres derived from Ni-metal organic framework for electromagnetic wave absorption. *Chem Eng J* 2020 383: 123207.
13. Yang HB, Wen B, Wang L. Carbon nanotubes modified CoZn/C composites with rambutan-like applied to electromagnetic wave absorption. Appl Surf Sci. 2020;509:145336.
14. Peng SS, Wang SY, Hao GZ, et al. Preparation of magnetic flower-like carbon-matrix composites with efficient electromagnetic wave absorption properties by carbonization of MIL-101(Fe). J Magn Magn Mater. 2019;487:165306.
15. Wang KF, Chen YJ, Tian R, et al. Liu, Porous Co-C core-shell nanocomposites derived from Co-MOF-74 with enhanced electromagnetic wave absorption performance. ACS Appl Mater Inter 2018 10: 11333–42.
16. Yan J, Huang Y, Yan YH, et al. High-performance electromagnetic wave absorbers based on two kinds of nickel-based MOF-derived Ni@C microspheres. ACS Appl Mater Inter. 2019;11:40781–92.
17. Veksha A, Yin K, Moo JGS, et al. Processing of flexible plastic packaging waste into pyrolysis oil and multi-walled carbon nanotubes for electrocatalytic oxygen reduction. J Hazard Mater. 2020;387:121256.
18. Santos JPF, Arjmand M, Melo GHF, et al. Electrical conductivity of electrospun nanofiber mats of polyamide 6/polyaniline coated with nitrogen-doped carbon nanotubes. Mater Design. 2018;141:333–41.

19. Ning MQ, Li JB, Kuang BY, et al. One-step fabrication of N-doped CNTs encapsulating M nanoparticles (M = Fe, Co, Ni) for efficient microwave absorption. Appl Surf Sci. 2018;447:244–53.
20. Hu QM, Yang RL, Mo ZC, et al. Nitrogen-doped and Fe-filled CNTs/$NiCo_2O_4$ porous sponge with tunable microwave absorption performance. Carbon. 2019;153:737–44.
21. Li XH, Wang L, You WB, et al. Enhanced microwave absorption performance from abundant polarization sites of ZnO nanocrystals embedded in CNTs via confined space synthesis. Nanoscale. 2019;11:22539–49.
22. Yin YC, Liu XF, Wei XJ, et al. Magnetically aligned Co-C/MWCNTs composite derived from MWCNT-interconnected zeolitic imidazolate frameworks for a lightweight and highly efficient electromagnetic wave absorber. ACS Appl Mater Inter. 2017;9:30850–61.
23. Xu XQ, Ran FT, Fan ZM, et al. Cactus-inspired bimetallic metal-organic framework-derived 1D-2D hierarchical Co/N-decorated carbon architecture toward enhanced electromagnetic wave absorbing performance. ACS Appl Mater Inter. 2019;11:13564–73.
24. Dai JJ, Yang HB, Wen B, et al. Flower-like MoS_2@$Bi_2Fe_4O_9$ microspheres with hierarchical structure as electromagnetic wave absorber. Appl Surf Sci. 2019;479:1226–35.
25. Zou F, Chen YM, Liu K, et al. Metal organic frameworks derived hierarchical hollow NiO/Ni/graphene composites for lithium and sodium storage. ACS Nano. 2016;10:377–86.
26. Zhu JN, Zhu XQ, Cheng FF, et al. Preparing copper doped carbon nitride from melamine templated crystalline copper chloride for fenton-like catalysis. Appl Catal B-Environ. 2019;256:117830.
27. An CH, Liu G, Li L, et al. In situ synthesized one-dimensional porous Ni@C nanorods as catalysts for hydrogen storage properties of MgH_2. *Nanoscale* 2014 6: 3223–3230.
28. Liu DW, Du YC, Xu P, et al. Waxberry-like hierarchical Ni@C microspheres with high-performance microwave absorption. J Mater Chem C. 2019;7:5037–46.
29. Lv ZM, Fan QH, Xie Y, et al. MOFs-derived magnetic chestnut shell-like hollow sphere NiO/Ni@C composites and their removal performance for arsenic(V). Chem Eng J. 2019;362:413–21.
30. Wang ZH, Xiong XQ, Qie L, et al. High-performance lithium storage in nitrogen-enriched carbon nanofiber webs derived from polypyrrole. Electrochim Acta. 2013;106:320–6.
31. Du YC, Liu WW, Qiang R, et al. Shell thickness-dependent microwave absorption of core-shell Fe_3O_4@C composites. *ACS Appl Mater & Inter* 2014 **6**: 12997–13006.
32. Xu JX, Qi YH, Wang L. In situ derived Ni_2P/Ni encapsulated in carbon/g-C_3N_4 hybrids from metal-organic frameworks/g-C_3N_4 for efficient photocatalytic hydrogen evolution. Appl Catal B-Environ. 2019;246:72–81.
33. Zhu T, Chang S, Song YF, Lahoubi M, et al. PVP-encapsulated $CoFe_2O_4$/rGO composites with controllable electromagnetic wave absorption performance. Chem Eng J. 2019;373:755–66.
34. Wu Q, Zhao RY, Zhu JF, et al. Interfacial improvement of carbon fiber reinforced epoxy composites by tuning the content of curing agent in sizing agent. Appl Surf Sci 2020 504: 144384.

35. Sheng ZH, Shao L, Chen JJ, et al. Catalyst free synthesis of nitrogen-doped graphene via thermal annealing graphite oxide with melamine and its excellent electrocatalysis. ACS Nano. 2011;5:4350–8.
36. Liu PB, Zhang YQ, Yan J, et al. Synthesis of lightweight N-doped graphene foams with open reticular structure for high-efficiency electromagnetic wave absorption. *Chem Eng J* 2019 **368**: 285–298.
37. Kenney MJ, Gong M, Li Y, et al. High performance silicon photoanodes passivated with ultrathin nickel films for water oxidation. Science. 2013;342:836–40.
38. Chen N, Mu GH, Pan XF, et al. Microwave absorption properties of $SrFe_{12}O_{19}/ZnFe_2O_4$ composite powders. Mater Sci Eng B- Adv. 2007;139:256–60.
39. Li D, Lin Y, Zhang M, et al. Achieved ultrahigh energy storage properties and outstanding charge–discharge performances in $(Na_{0.5}Bi_{0.5})_{0.7}Sr_{0.3}TiO_3$-based ceramics by introducing a linear additive. Chem Eng J. 2020;392:123729.
40. Lin Y, Li D, Zhang M, et al. $(Na_{0.5}Bi_{0.5})_{0.7}Sr_{0.3}TiO_3$ modified by $Bi(Mg_{2/3}Nb_{1/3})O_3$ ceramics with high energy-storage properties and an ultrafast discharge rate. J Mater Chem C. 2020;8:2258–64.
41. Yang HB, Liu PF, Yan F, et al. A novel lead-free ceramic with layered structure for high energy storage applications. J Alloy Compd. 2019;773:244–9.
42. Liu XY, Yang HB, Yan F, et al. Enhanced energy storage properties of $BaTiO_3$-$Bi_{0.5}Na_{0.5}TiO_3$ lead-free ceramics modified by $SrY_{0.5}Nb_{0.5}O_3$. J Alloy Compd. 2019;778:97–104.
43. Wu ND, Liu XG, Zhao CY, et al. Effects of particle size on the magnetic and microwave absorption properties of carbon-coated nickel nanocapsules. *J Alloy Compd* 2016 656: 628–634.
44. Wang YF, Chen DL, Yin X, et al. Hybrid of MoS_2 and reduced graphene oxide: a lightweight and broadband electromagnetic wave absorber. ACS Appl Mater Inter. 2015;7:26226–34.
45. Wang HC, Xiang L, Wei W, et al. Efficient and lightweight electromagnetic wave absorber derived from metal organic framework-encapsulated cobalt nanoparticles. ACS Appl Mater Inter. 2017;9:42102–10.
46. Qiang R, Du YC, Zhao HT, et al. Metal organic framework-derived Fe/C nanocubes toward efficient microwave absorption. J Mater Chem A. 2015;3:13426–34.
47. Lu SB, Meng Y, Wang HB, et al. Great enhancement of electromagnetic wave absorption of MWCNTs@ carbonaceous CoO composites derived from MWCNTs-interconnected zeolitic imidazole framework. *Appl Surf Sci* 2019 **481**: 99–107.
48. Yang R, Yuan JQ, Yu CH, et al. Efficient electromagnetic wave absorption by SiC/Ni/NiO/C nanocomposites. J Alloy Compd. 2020;816:152519.
49. Zhou CL, Wang XX, Luo H, et al. Rapid and direct growth of bipyramid TiO_2 from $Ti_3C_2T_x$ MXene to prepare $Ni/TiO_2/C$ heterogeneous composites for high-performance microwave absorption. Chem Eng J. 2020;383:123095.
50. Zhang N, Li JF, Men XS, et al. Cleaning synthesis of core-shell structured Ni@PPy composite as excellent lightweight electromagnetic wave absorber. J Mate Sci-Mater El. 2019.

DOI:10.1007/s10854-019-02663-5.

51. Li N, Xie X, Lu HX, et al. Novel two-dimensional $Ti_3C_2T_x$/Ni-spheres hybrids with enhanced microwave absorption properties. Ceram Int. 2019;45:22880–8.
52. Huang LN, Chen CG, Huang XY, et al. Enhanced electromagnetic absorbing performance of MOF-derived Ni/NiO/Cu@C composites. Compos Part B-Eng. 2019;164:583–9.

Figures

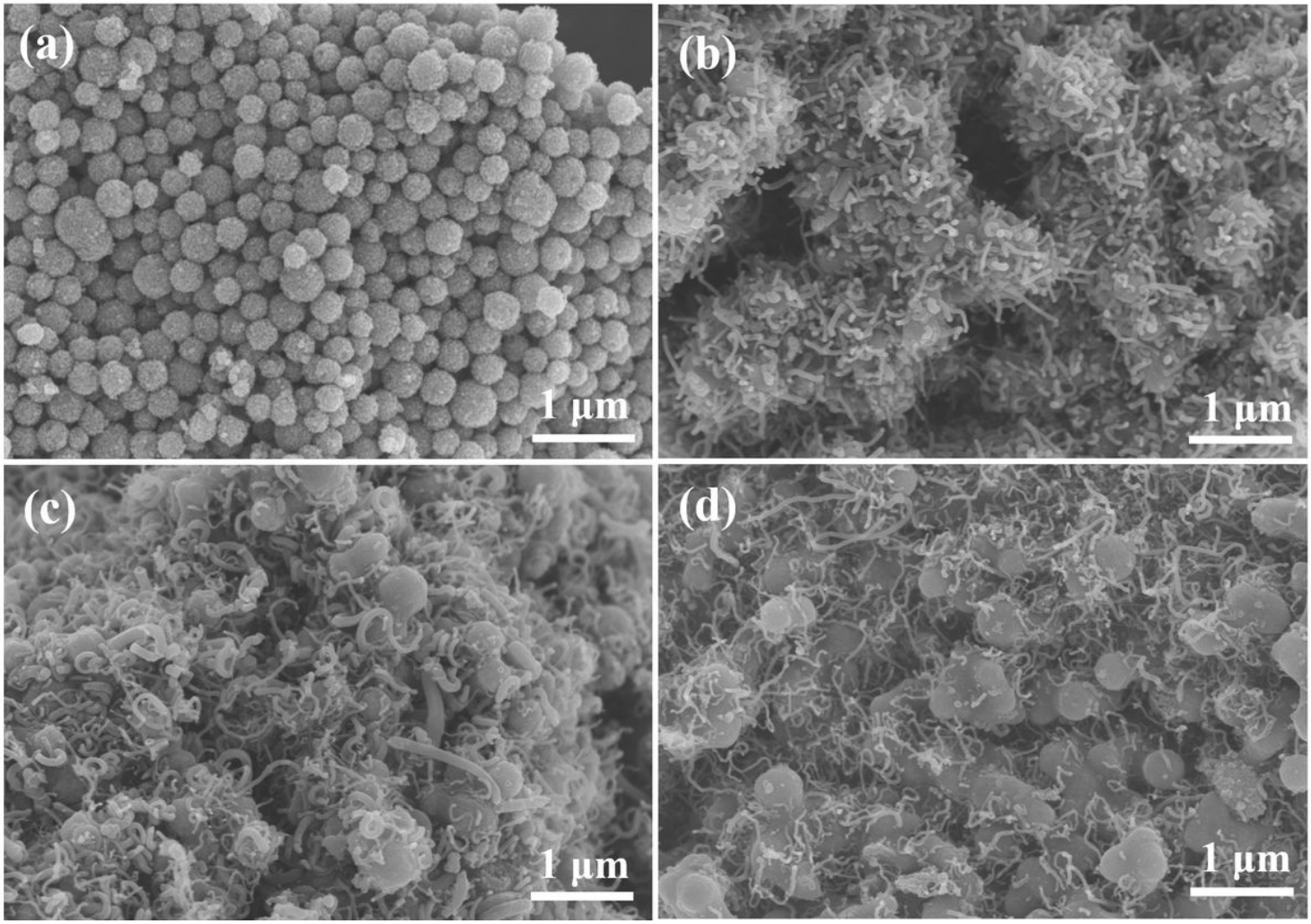

Figure 1

SEM images of (a) Ni/C, (b) Ni-C/CNTs-1, (c) Ni-C/CNTs-2 and (d) Ni-C/CNTs-3 composites.

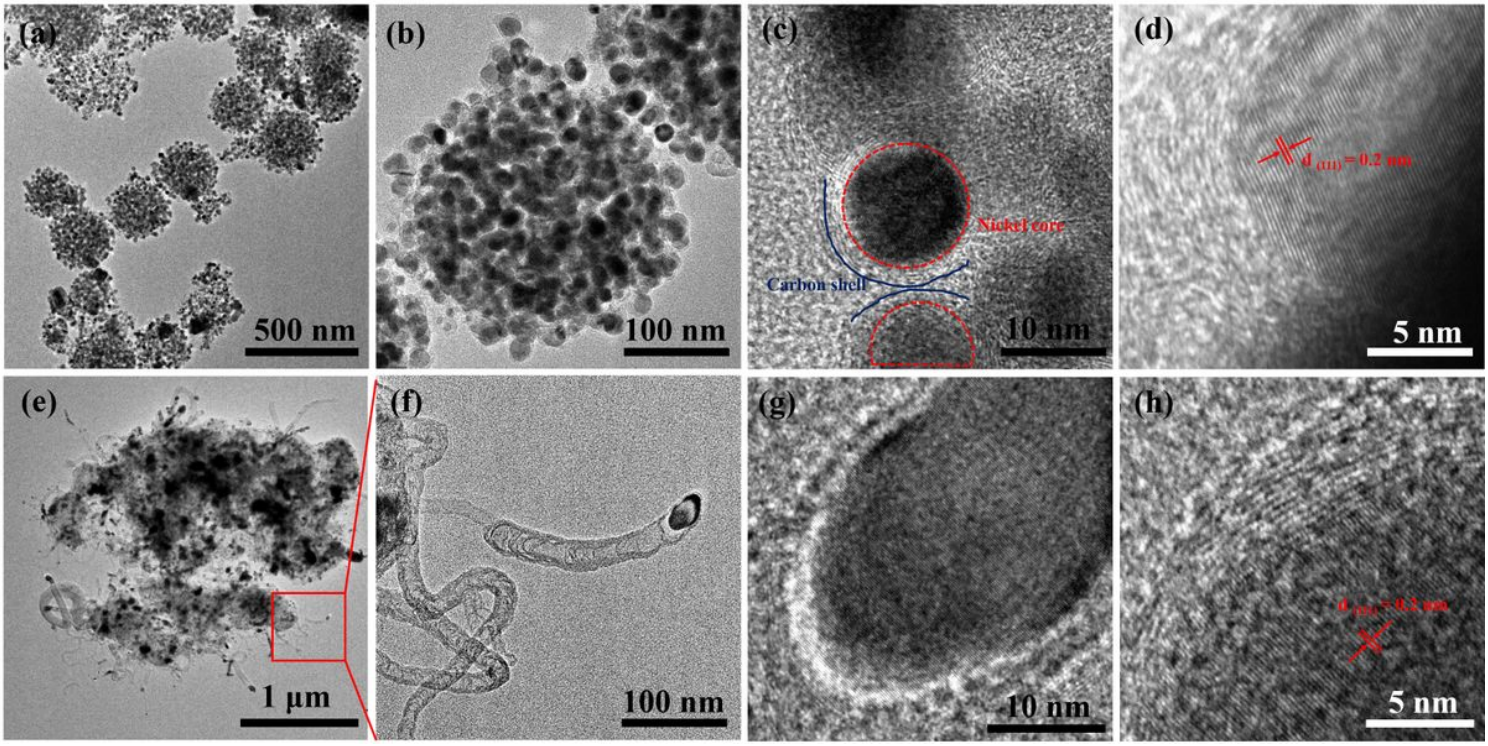

Figure 2

TEM and HR-TEM images of (a-d) Ni/C and (e-h) Ni-C/CNTs-2 composites.

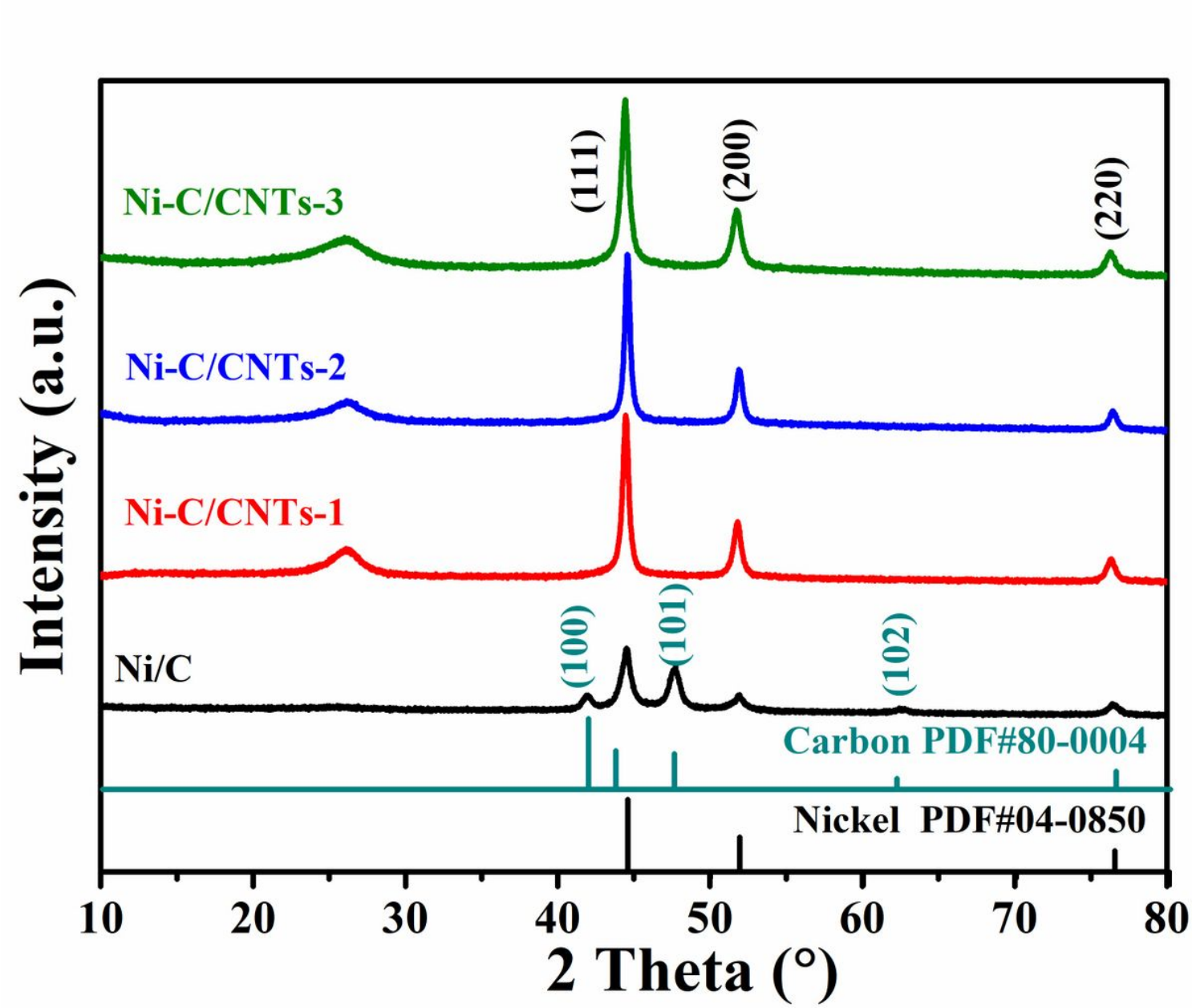

Figure 3

XRD patterns of Ni/C, Ni-C/CNTs-1, Ni-C/CNTs-2 and Ni-C/CNTs-3 composites.

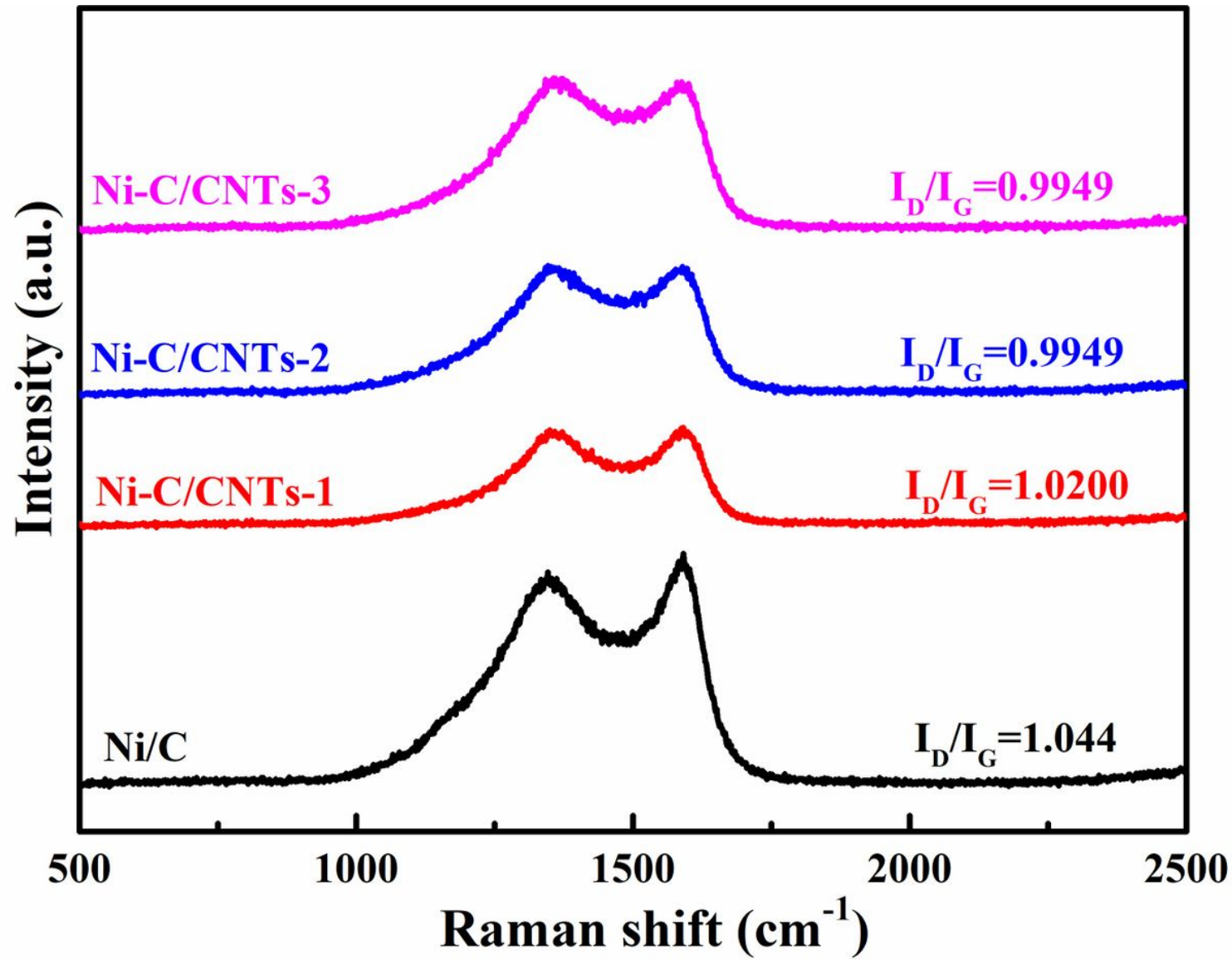

Figure 4

Raman spectra of Ni/C, Ni-C/CNTs-1, Ni-C/CNTs-2 and Ni-C/CNTs-3 composites.

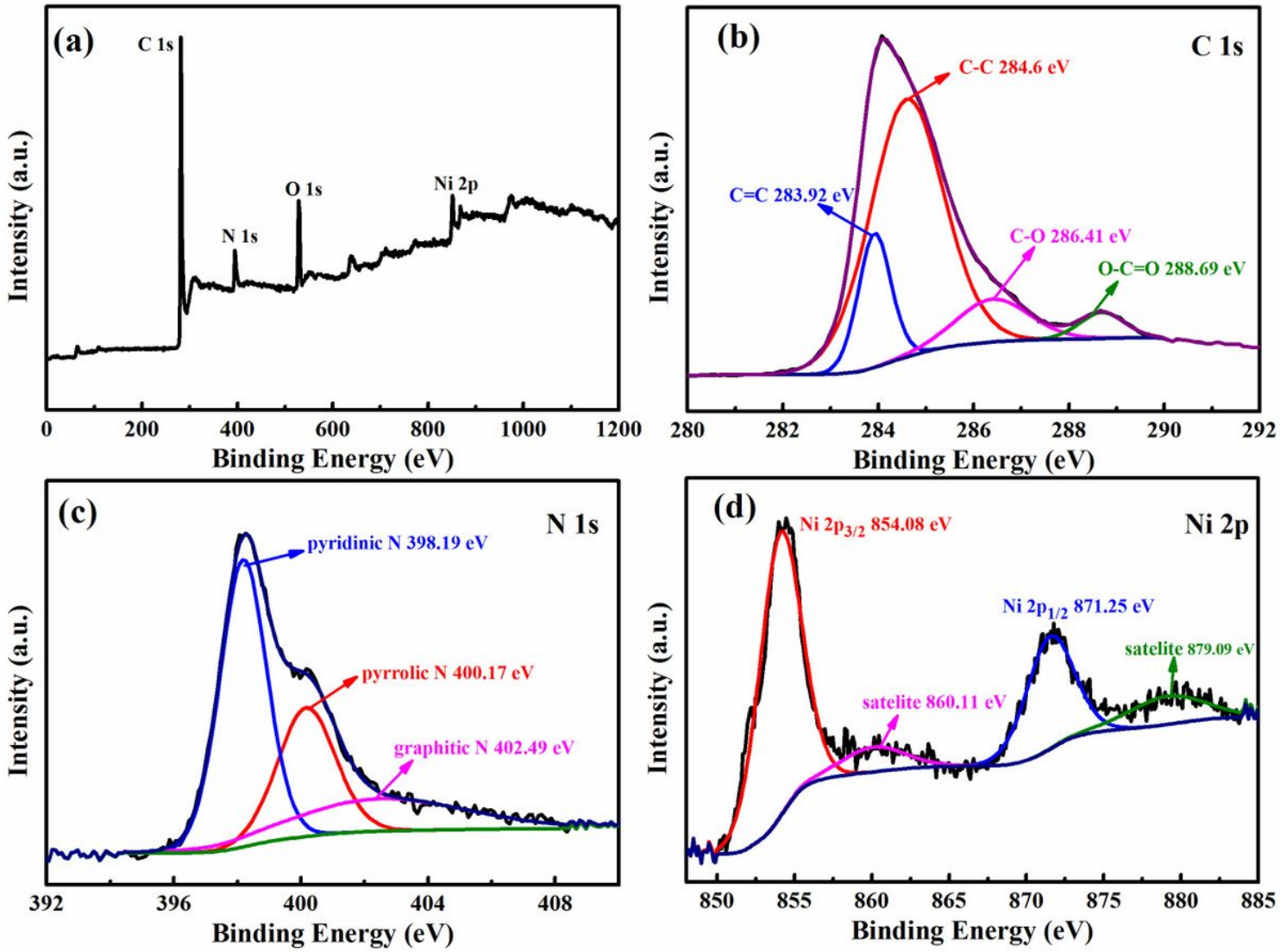

Figure 5

(a) XPS survey spectrum, (b) C 1s spectrum, (c) N 1s spectrum (d) Ni 2p spectrum of Ni-C/CNTs-2 composite.

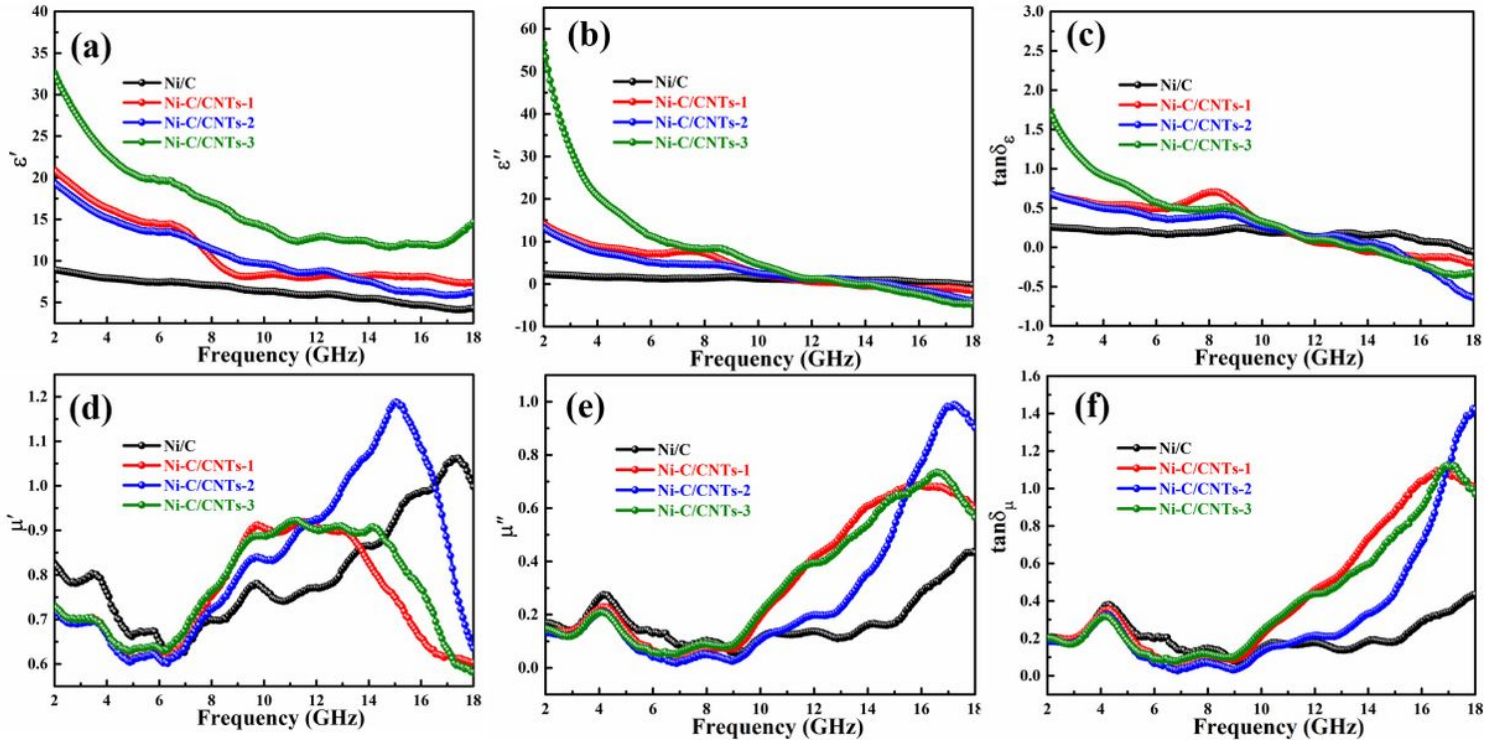

Figure 6

Frequency dependence of electromagnetic parameters of Ni/C and Ni-C/CNTs composites: (a) the real part (ε'), (b) imaginary part (ε"), (c) dielectric loss (tanδε), (d) real part (μ'), (e) imaginary part (μ"), and (f) magnetic loss (tanδμ).

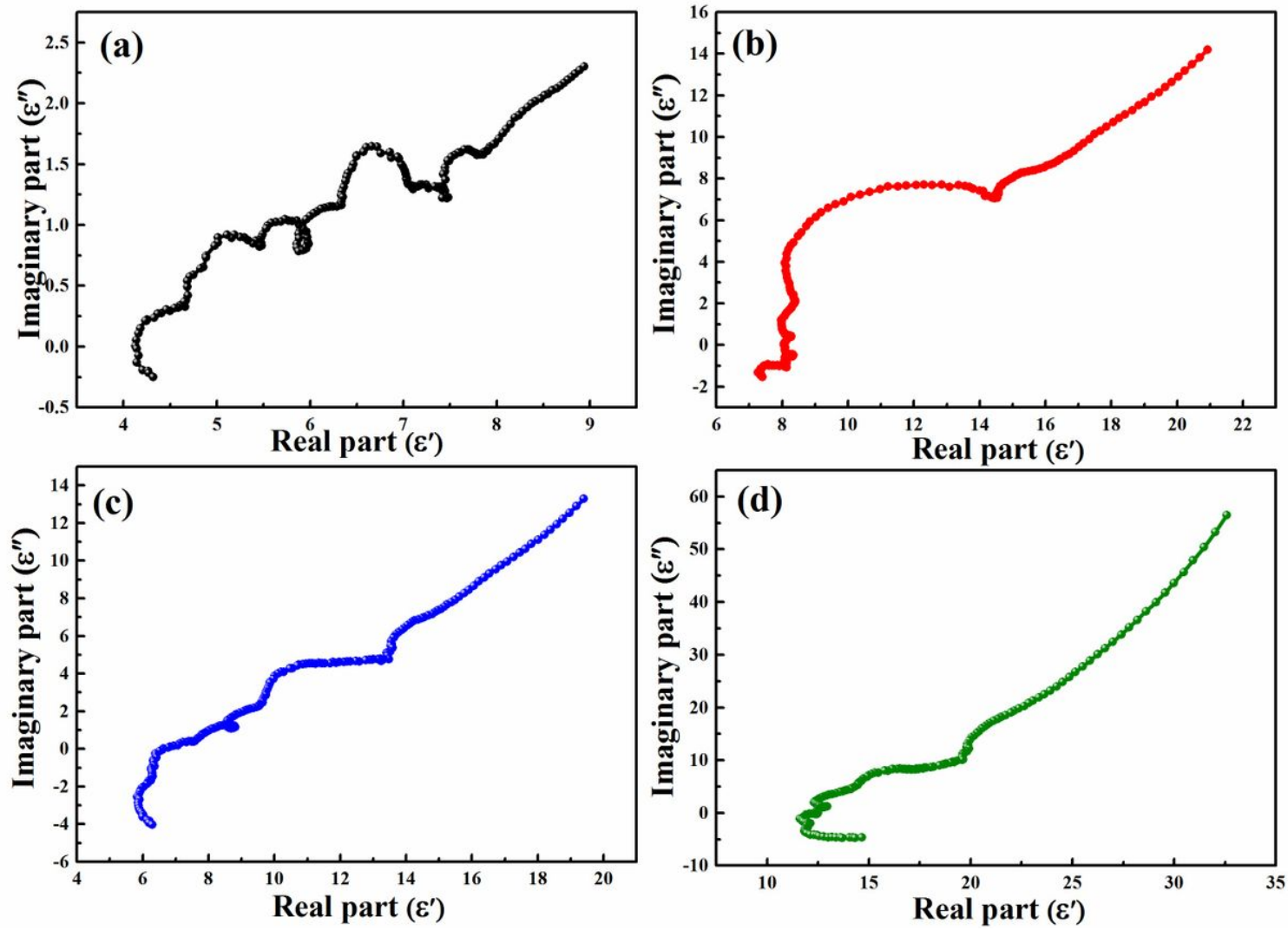

Figure 7

Cole-Cole semicircles for (a) Ni/C, (b) Ni-C/CNTs-1, (c) Ni-C/CNTs-2, and (d) Ni-C/CNTs-3 composites in the frequency range of 2-18 GHz.

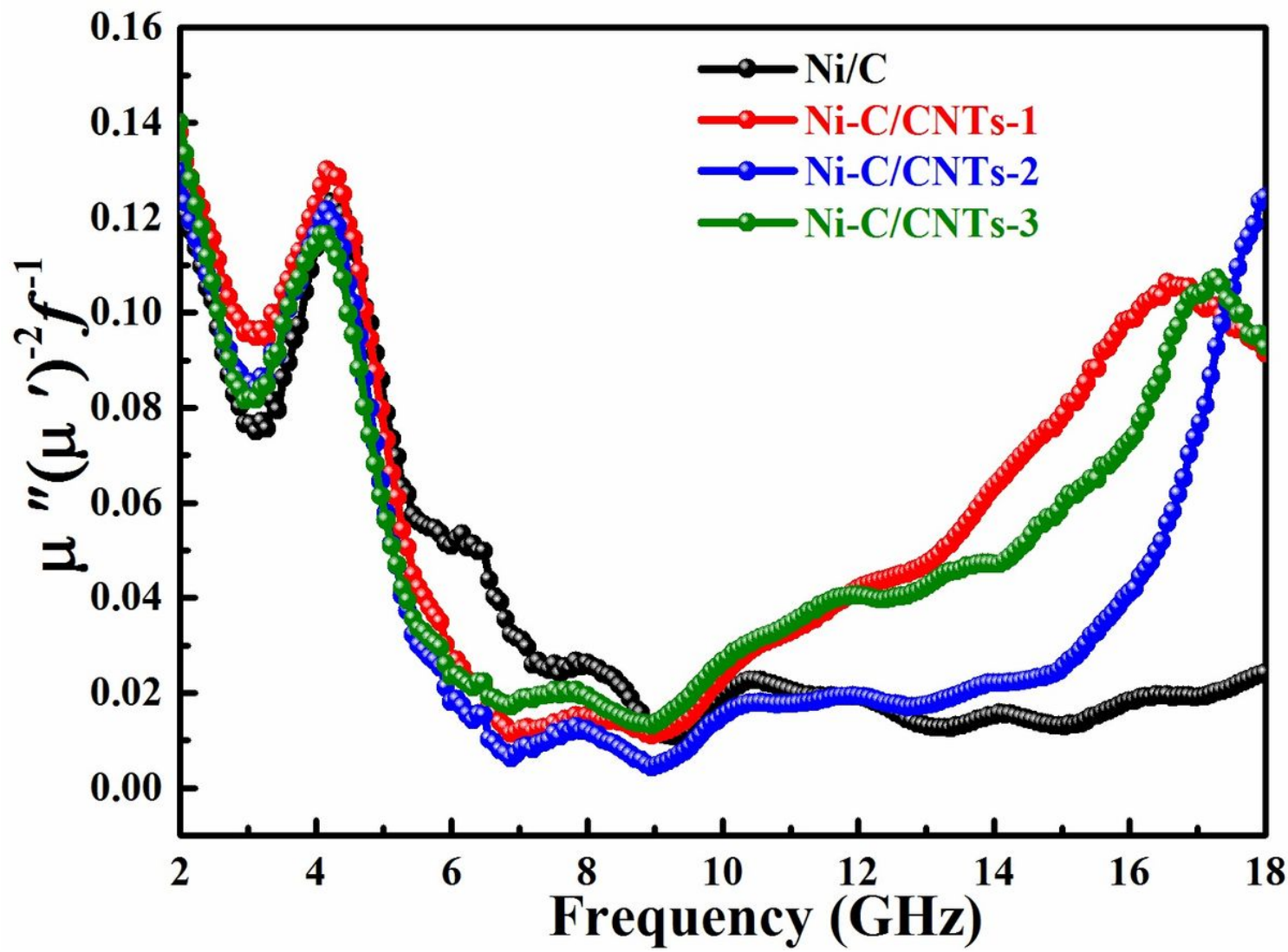

Figure 8

μ"(μ')-2f-1 versus frequency curves of Ni/C, Ni-C/CNTs-1, Ni-C/CNTs-2 and Ni-C/CNTs-3 composites.

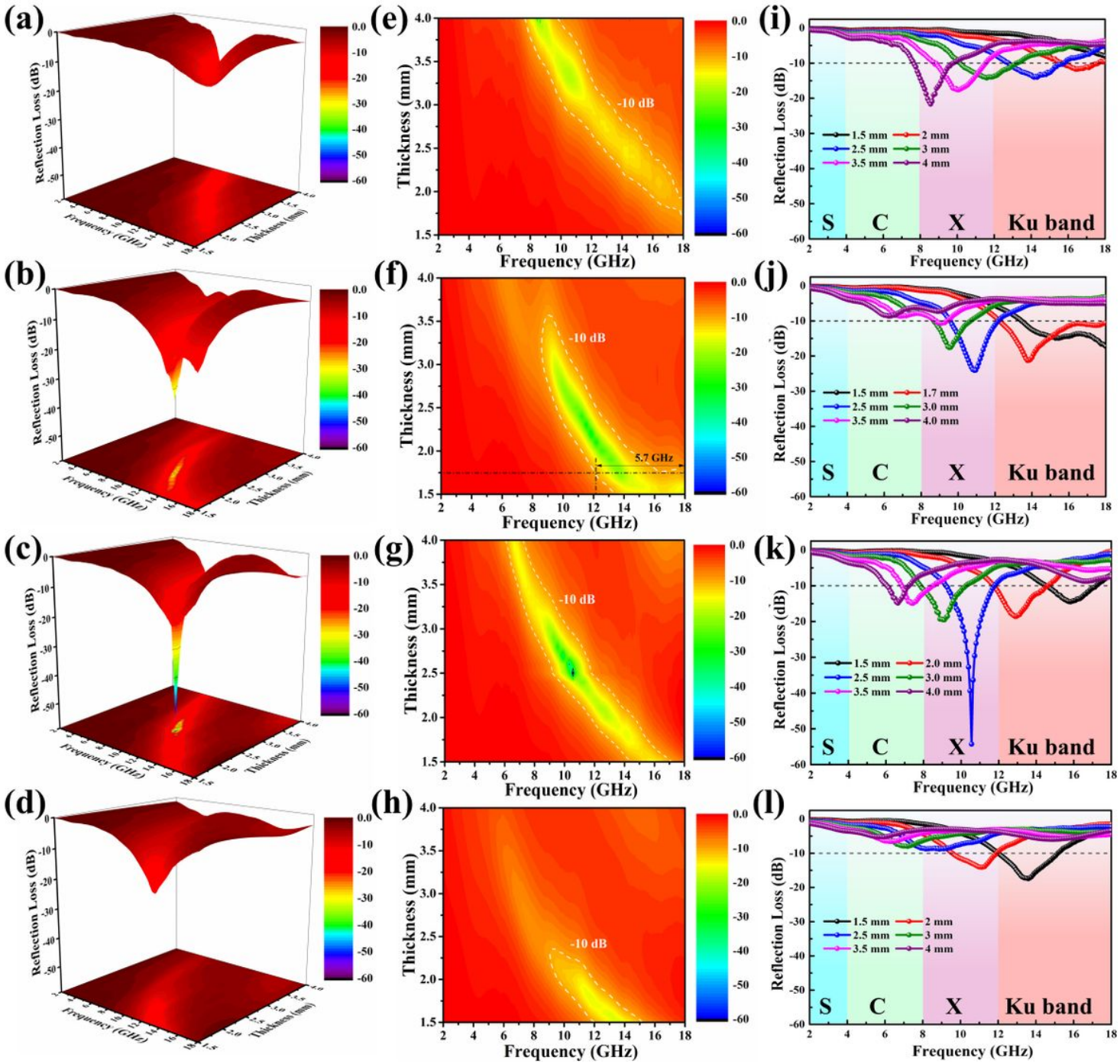

Figure 9

3D RL, 3D projection plots, and RL values of (a, e, i)Ni/C, (b, f, j)Ni-C/CNTs- 1, (c, g, k) Ni-C/CNTs-2, (d, h, l)Ni-C/CNTs-3 composites.

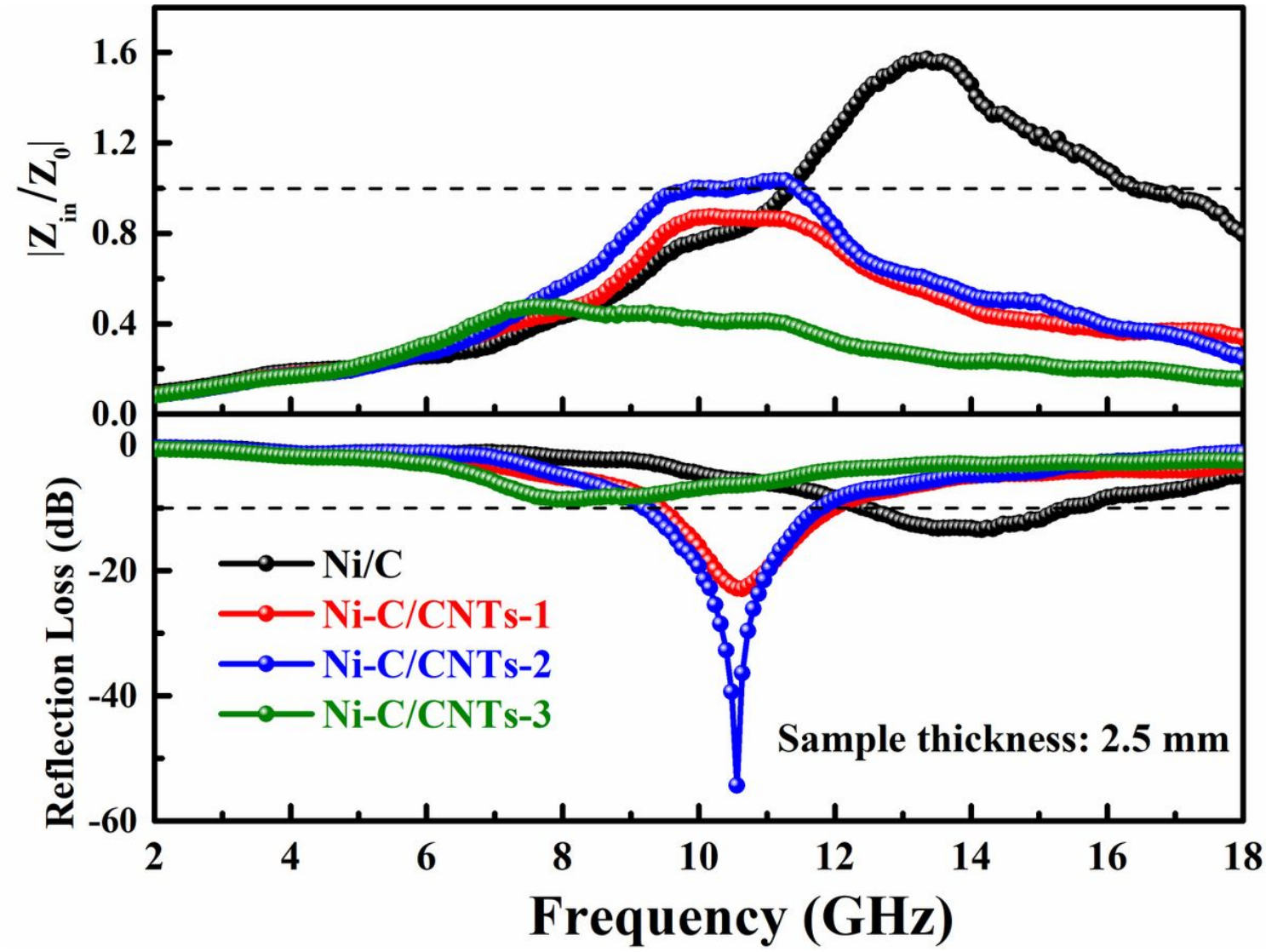

Figure 10

Comparison of relative input impedance (Zin/Z0) and RL curves.

Supplementary Files

This is a list of supplementary files associated with this preprint. Click to download.

- Scheme1.tif
- Scheme1.tif
- Scheme1.tif
- Scheme2.tif
- Scheme2.tif
- Scheme2.tif
- Figurecaption.docx

- Figurecaption.docx
- Figurecaption.docx